frontiers in Materials

ORIGINAL RESEARCH
published: 01 November 2021
doi: 10.3389/fmats.2021.761236

Construction of Concave PdAg Nanoshells with Limited Thickness for Efficient Electroxidation of Ethanol

Quanlin Wu[1], Gongguo Zhang[2], Na Zhao[2], Yiqun Zheng[2], Yanyun Ma[3]*, Feng Liu[4] and Maochang Liu[4]*

[1]School of Engineering, Jining University, Qufu, China, [2]School of Chemistry, Chemical Engineering, and Materials, Jining University, Qufu, China, [3]Jiangsu Key Laboratory for Carbon-Based Functional Materials & Devices, Institute of Functional Nano & Soft Materials (FUNSOM), Soochow University, Suzhou, China, [4]International Research Center for Renewable Energy, National Key Laboratory of Multiphase Flow in Power Engineering, Xi'an Jiaotong University, Xi'an, China

Noble metal nanocrystals enclosed with curved surfaces are of great benefit for applications in electrocatalysis since the atomic steps and kinks on these facets have higher chemical activity. Herein, we report the fabrication of PdAg nanoshells with tunable thickness in the range of 5–13 nm and a unique concave cubic morphology, as well as the exploration of their applications for ethanol oxidation reaction (EOR) in alkaline media. The success of current work relies on the conformal deposition of PdAg on concave Au nanocubes, where the controlled reaction kinetics and proper chosen capping agent are both crucial for the growth mode. When loaded on carbon black and working as electrocatalysts, they exhibited superb electrochemical activity (e.g., 600.21 mA mg^{-1} in mass activity and 19.57 A m^{-2} in specific activity), together with improved EOR kinetics and long-term durability, as compared to Au@Pd nanoparticles and commercial Pd/C. The current work offers a feasible strategy to produce PdAg bimetallic nanocrystals with concave surface and validates their promising application as fuel cell catalysts, which could be extended to morphology engineering of other noble-metal nanocrystals for a broad range of applications.

Keywords: ethanol oxidation reaction, seeded growth, nanocrystal, bimetallic, concave

OPEN ACCESS

Edited by:
Zsolt Pap,
University of Szeged, Hungary

Reviewed by:
Sang-Il Choi,
Kyungpook National University, South Korea
Albert Serrà,
University of Barcelona, Spain

****Correspondence:***
Yiqun Zheng
whzyq@163.com
Yanyun Ma
mayanyun@suda.edu.cn

Specialty section:
This article was submitted to Colloidal Materials and Interfaces, a section of the journal Frontiers in Materials

Received: *19 August 2021*
Accepted: *22 September 2021*
Published: *01 November 2021*

Citation:
Wu Q, Zhang G, Zhao N, Zheng Y, Ma Y, Liu F and Liu M (2021) Construction of Concave PdAg Nanoshells with Limited Thickness for Efficient Electroxidation of Ethanol. Front. Mater. 8:761236. doi: 10.3389/fmats.2021.761236

INTRODUCTION

Ethanol oxidation reaction is one of the important classes of cathodic reaction for fuel cells that converts the chemical energy stored in liquid fuel to electricity(Mann et al., 2006; An and Zhao, 2011; Hong et al., 2019; Kim et al., 2019; Kim et al., 2020; Kabiraz et al., 2021). Compared to the commercial device directly using gaseous hydrogen as the hydrogen sources, ethanol can be of higher energy density and bio-renewability, as well as the advantage with respect to storage and transportation under ambient condition (Lamy et al., 2001; Shen et al., 2012). Previous studies focusing on the detailed mechanistic and kinetic understanding of the processes have suggested that the dehydrogenation of the ethanol occurs quickly and the rate-determining step is the oxidative removal of the radicals by the hydroxide ions (Wang et al., 2004; Liang et al., 2009; Ishimoto et al., 2013). To accelerate the kinetics of such process, typical commercial electrocatalysts for alkaline media are fabricated using carbon black supported tiny Pd nanoparticles(Antolini, 2007). Moreover, the alloying of Pd with other metals and/or modification with non-metal elements could be a feasible strategy to improve

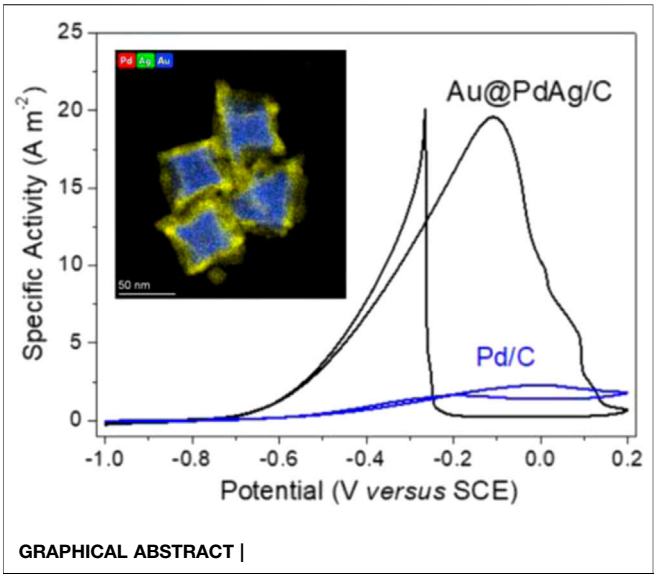

GRAPHICAL ABSTRACT |

the electrochemical performance since it can tune the surface affinity towards key intermediates to achieve the maxima electrocatalytic activity along the volcano-type plot as a function of the heat of adsorption and also enhanced anti-poisoning ability of the electrocatalyst (Zhang et al., 2016b). To this end, the electrochemical activity of many metal combinations, such as PdAu (Feng et al., 2013; Hong et al., 2014; Yang et al., 2017), PdPt (Dutta et al., 2016), PdAg (Lu and Chen, 2012; Peng et al., 2015; Bin et al., 2016; Fang et al., 2018; Lv et al., 2019; Yang et al., 2020a; You et al., 2020; Cui et al., 2021; Nguyen et al., 2021), PdCu (Wang et al., 2012; Hu et al., 2014; Liu et al., 2015; Jiang et al., 2016; Yang et al., 2019; Jana et al., 2021), PdPtCu (Wang et al., 2020), and phosphorous-doped Pd-based nanocrystals (Liu et al., 2019; Yang et al., 2020b; Lv et al., 2020; Yu et al., 2020), have been extensively measured, where the underlying mechanisms are investigated using theoretical deduction (i.e., d-band center theory) and *in situ* techniques (i.e., *in situ* FTIR).

The incorporation of more than one types of noble metal atom in one nanoparticle allows the formation of a more complex structure, which would greatly enhance their properties, often making them superior to their monometallic counterparts (Zhang et al., 2016a; Gilroy et al., 2016). Such advance is of great value and importance in rational design of catalyst since the binding energy of catalyst surface and thus the catalytic performances are highly sensitive to the spatial arrangement and atomic ordering of different types of metallic atoms (Wang et al., 2016; Zhao et al., 2017; Fu et al., 2020). In the context of PdAg, the two metals can form a continuous solid solution, which makes their composition manipulation versatile (Li et al., 2011). Additionally, the underpotential-deposition (UPD) effect of Ag ions during the crystal growth can be potentially used to facilitate the *in situ* generation of Ag monolayer over the nanoparticle, serving as a "metallic" capping agent to specifically bind to and stabilize the crystal plane with high indexes (Langille et al., 2012). In this case, the resulting product would tend to exhibit a curved surface that normally unfavored by thermodynamics.

Thanks to research efforts from many groups, it is now possible to fabricate PdAg-based nanocrystals with a set of morphologies and controlled elemental composition. For example, mesoporous nanocrystals can be prepared using soft template methods (Stein et al., 2008; Li et al., 2013; Lahiri and Endres, 2017; Lahiri et al., 2020). Cheng and coworkers reported the fabrication of 2D PdAg alloy nanodendrites as a high-performance electrocatalyst for EOR, which are obtained *via* the co-reduction of Pd and Ag precursors in aqueous solution with the presence of octadecyltrimethylammonium chloride as the structural directing agent (Huang et al., 2018). Lee and coworkers reported the fabrication of porous Pd-Ag bimetallic dendrites by conducting galvanic replacement reaction between Ag dendrites and $Pd(NO_3)_2$ and studied the composition-dependent electrochemical activity towards EOR (Jo et al., 2016). Tsuji and coworkers reported that noble Au@PdAg and Au@PdAg@Ag core–shell nanorods (NRs) having PdAg alloy shells in the form of cuboids and dumbbell were synthesized using Au@Pd NRs as seeds (Tsuji et al., 2015). Despite of these successful demonstrations, the fabrication of PdAg nanocrystals with concave surface has achieved limited success (Wang et al., 2021). It is well-accepted that the concave surface usually involves the presence of multiple high-index facets, and thus atomic steps and kinks with low coordination numbers in high densities would be offered and working as active sites for the improvement of electrochemical activity (Tian et al., 2007; Xia et al., 2011).

Herein, we report a facile synthesis of PdAg nanoshells enclosed with concave surface *via* seeded growth. Starting with concave cubic Au nanocrystals as the seed, the sequential addition and reduction of Pd and Ag precursor allows the conformal growth to form concave PdAg shell with limited thickness. The value of current work mainly relies on the three following aspects: 1) for the first time, Au@PdAg nano-alloys with a concave cubic morphology are prepared in high purity and used as electrocatalysts for EOR; 2) The shell thickness of PdAg can be readily tuned in the range of 5.8–12.5 nm by simply changing the amount of Pd precursor used in seeded growth, without causing significant loss in concave surface feature; 3) The carbon-supported Au@PdAg core-shell concave nanocubes exhibited superb electrochemical activity (~10 fold in specific activity higher than that of commercial Pd/C), improved EOR kinetics, and long-term durability, revealing the contribution of curved surface and demonstrating their advantage in both structure and elemental composition.

EXPERIMENTAL DETAILS

Materials

Gold(III) chloride trihydrate ($HAuCl_4$ $3H_2O$, 99.9%), sodium tetrachloropalladate(II) (Na_2PdCl_4, 98%), silver nitrate ($AgNO_3$, 99%), cetyltrimethylammonium chloride (CTAC, 97%), cetyltrimethylammonium bromide (CTAB, 99%) and ascorbic acid (AA, 99.0%) were all obtained from Aladdin Chemical (Shanghai, China) and used as received. Docoscyltrimethylammonium chloride (DTAC, 85%) was obtained from Degussa and used as received. Commercial Pd/C (10 wt.% Pd loading, matrix activated carbon support) was obtained

TABLE 1 | Size information and synthetic parameters for Au@PdAg concave nanocubes with controlled thickness.

No	Shell thickness		DTAC (20 mM)	AA (10 mM)	Na_2PdCl_4 (20 mM)	$AgNO_3$ (2 mM)	Au seeds
	t (nm)	σ (nm)					
P1	5.8	1.9	3 ml	0.5 ml	5 ml	0.5 μL	0.5 ml
P2	7.8	3.0	3 ml	0.5 ml	10 ml	0.5 μL	0.5 ml
P3	8.8	3.4	3 ml	0.5 ml	20 ml	0.5 μL	0.5 ml
P4	9.9	4.6	3 ml	0.5 ml	50 ml	0.5 μL	0.5 ml
P5	12.5	4.9	3 ml	0.5 ml	100 ml	0.5 μL	0.5 ml

from Sigma-Aldrich and used as received. Conductive carbon black was obtained from Cabot and used as received. In all experiments, we used deionized water with a resistivity of 18.2 MΩ cm, which was prepared using an ultrapure water system (Ulupure, China).

Standard procedure for the Synthesis of Au@PdAg Core-shell Nanocrystals With concave Surface

Concave cubic Au seeds were generated according to the standard procedure as described in our previous study (Zhang et al., 2020). Typically, one batch of Au concave nanocubes were purified and re-dispersed in 1 ml of water for further use (mass concentration: ~0.15 mg_{Au}/mL). For the synthesis of Au@PdAg concave nanocubes (Procedure P1), aqueous solutions of DTAC (20 mM, 3 ml), as-prepared concave Au cubic seeds (0.5 ml), Na_2PdCl_4 (20 mM, 5 μL), AA (10 mM, 0.5 ml) were sequentially mixed in a 20-ml glass vial and aged for 10 min at room temperature, followed by the injection of $AgNO_3$ (2 mM, 0.5 ml) solution. The reaction proceeded for 2 h in a water bath set at 60°C and the products were collected *via* centrifugation and washed with water once prior to further use. See **Table 1** for synthetic details for Au@PdAg core-shell concave nanocubes with different PdAg shell thickness (Procedure P1~P5). For Au@Pd nanoparticles used in electrocatalysis, they were produced *via* the procedure P5, except that no $AgNO_3$ was added.

Instrumentations and Characterizations

Transmission electron microscopy (TEM), high-resolution TEM (HRTEM), selected-area electron diffraction (SAED), high angle annular dark field-scanning transmission electron microscopy (HAADF-STEM) and EDX (energy dispersive X-ray)-STEM mapping images were obtained using a Talos F200X (FEI, USA) microscope operated at 200 kV accelerating voltage. Scanning electron microscopy (SEM) images were obtained using a Zeiss Ultra60 microscope operated at 12 kV. The crystalline structures were analyzed

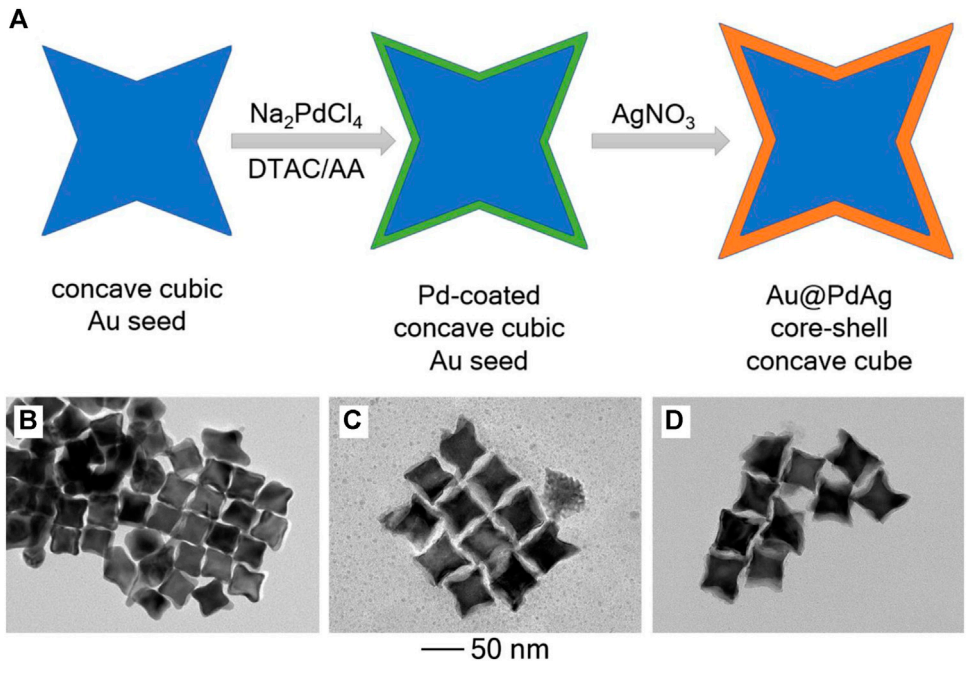

FIGURE 1 | (A) Schematic illustration showing the construction of Au@PdAg core-shell concave nanocubes by conducting sequential conformal growth of Pd and Ag over concave Au cubic seeds. **(B–D)** TEM images: **(B)** concave cubic Au seeds; **(C)** Pd-coated concave Au nanocubes; **(D)** Au@PdAg core-shell concave nanocubes.

with a MiniFlex600 X-ray diffractometer (XRD, Rigaku). X-ray photoelectron spectroscopy (XPS) measurements were performed using a Thermo Fisher Scientific KALPHA XPS with monochromatic Al K_α radiation ($h\nu$ = 1,486.6 eV). All extinction spectra were recorded using a T9 dual-beam UV-vis-NIR spectrometer (PERSEE, China). Inductively coupled plasma analysis was conducted on an ICAP-5000 inductively coupled plasma optical emission spectrometer (Focused Photonics Instrument, China). EOR measurement was carried out in a standard three-electrode system controlled by a CHI-760E potentiostat (CHInstruments, China). See supporting information for operational details.

RESULTS AND DISCUSSION

Conformal Deposition of PdAg Over Concave Au Nanocubes

Typical synthesis started with the preparation of concave Au nanocubes in high purity according to the method described in our previous study (Zhang et al., 2020), followed by purification and the use as seeding material. The growth process involved the use of DTAC and AA as the capping agent and reductant, respectively, as well as the sequential addition of Pd and Ag precursor, respectively (**Figure 1A**). TEM image of the Au seeds showed that they had the concave cubic shape in high uniformity, together with an average edge length of 37 nm (**Figure 1B**). The Au@Pd and Au@PdAg products obtained *via* the sequential addition, respectively, maintained the concave cubic morphology as seeds, indicating the successful conformal growth occurred (**Figures 1C,D**). It is worth noting that the absence of Pd precursor would lead to the formation of Au@Ag core-shell nanocubes with the truncations on the corners (**Supplementary Figure S1A**). The position of concave cubic Au seeds was not located in the right center of the resulting nanocube, which should be attributed to the fact that heterogenous nucleation and growth of Ag initially occurred to one or partial side faces of the concave cubic Au seeds (Zhu et al., 2012). Corresponding UV-vis extinction spectrum showed that the Au@Ag core-shell nanocubes exhibited the major peak located at 501 nm, together with a shoulder peak located at around 400 nm (**Supplementary Figure S1B**).

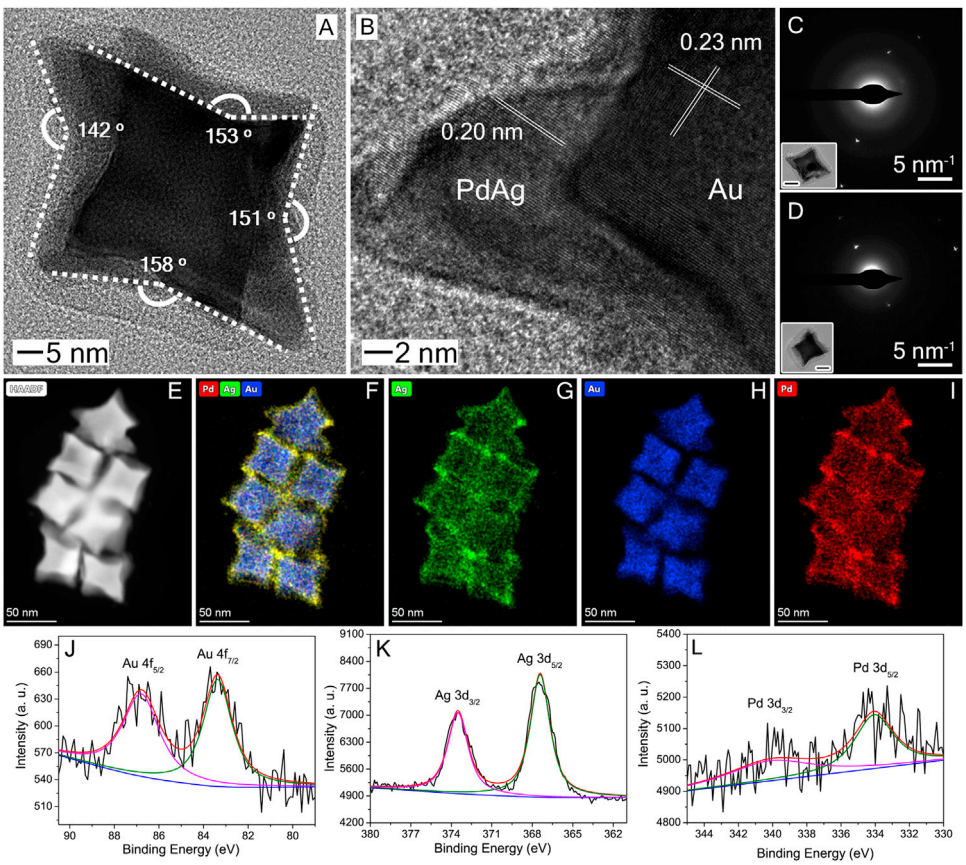

FIGURE 2 | Morphology and structural characterizations of Au@PdAg core-shell concave nanocubes: **(A)** TEM; **(B)** HRTEM; **(C, D)** SAED; **(E)** HAADF-STEM; **(F–I)** EDX-STEM elemental mapping: **(F)** overlap of Au, Pd, and Ag, **(G)** Ag, **(H)** Au, **(I)** Pd; **(J–L)** XPS spectra: **(J)** Au 4f; **(K)** Ag 3d; **(L)** Pd 3d. The insets in **(C, D)** shows the corresponding particle, with a scale bar of 10 nm.

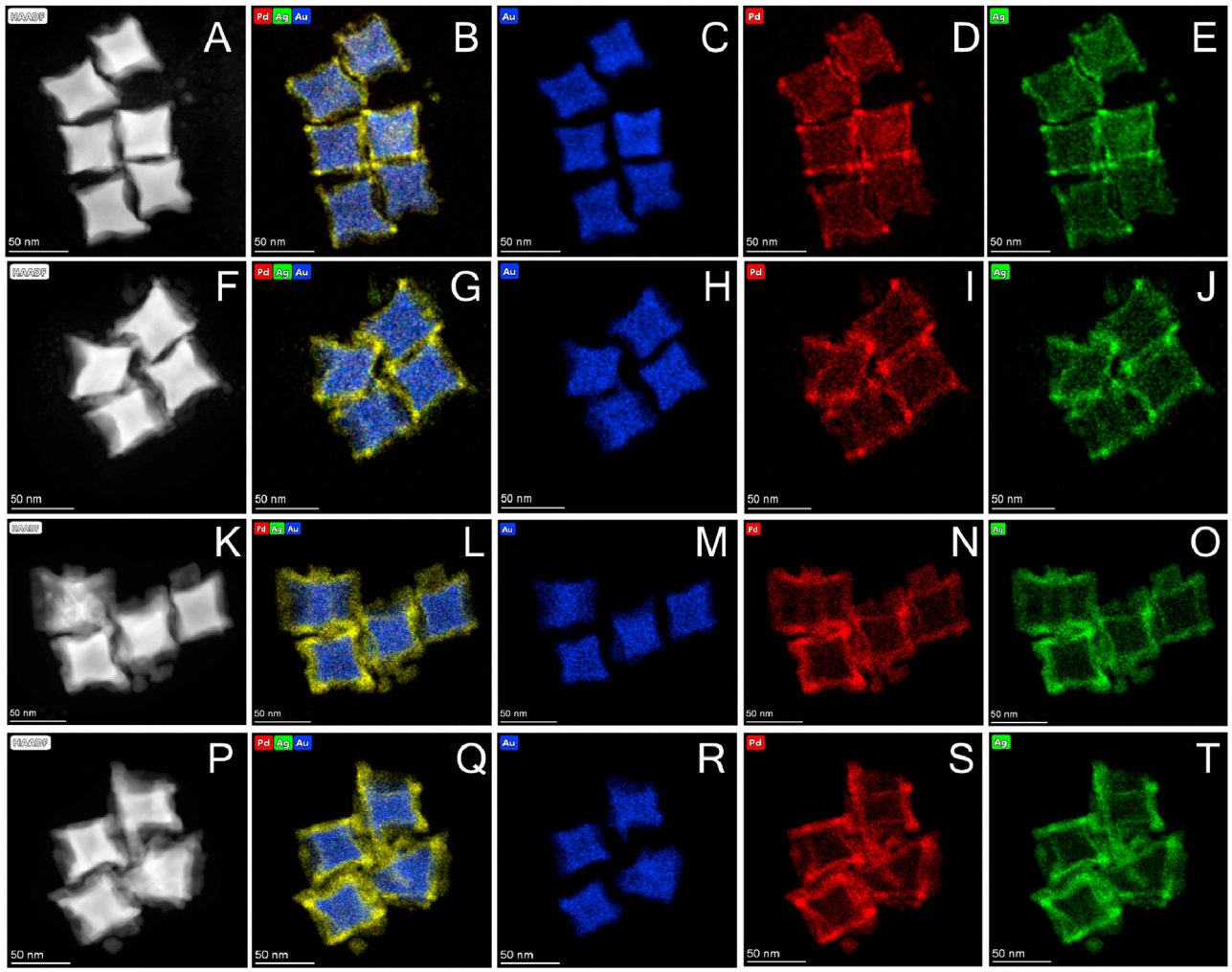

FIGURE 3 | Morphology and characterizations of Au@PdAg core-shell concave nanocubes with different thickness of PdAg shell: **(A–E)** 7.8 nm; **(F–J)** 8.8 nm; **(K–O)** 9.9 nm; **(P–T)** 12.5 nm, respectively. The images in **(A, F, K, and P)** were HAADF-STEM and the rest were EDX-STEM: **(B, G, L, and Q)** overlap of Au, Pd, and Ag, **(C, H, M, and R)** Au, **(D, I, N, and S)** Pd, **(E, J, O, and T)** Ag.

Morphology and Structure Characterizations

To further analyze their morphology and structure, a set of characterizations, including HRTEM, SAED, HAADF-STEM, EDX-STEM, and XPS, were conducted. As shown in **Figure 2A**, the TEM image of an individual particle clearly shows the concave feature on the particle surface. Curved projections could be observed at several different facets, projection angle was estimated to between 142°, 151°, 153°, and 158°, respectively. Considering these projection angles are the angles between the projection line of exposed facets, several typical high-index facets, such as {730}, {830}, {920}, and {720} facets, could be calculated and indexed (Yu et al., 2010; Zhang et al., 2015; Kuo et al., 2018; Luo et al., 2019). The HRTEM image (**Figure 2B**) shows lattice fringes at the corner region, where a clear boundary could be observed to differentiate the Au and PdAg part. The lattice spacing of 0.23 and 0.20 nm, can be ascribed to the (111) crystal plane of Au and PdAg, respectively. SAED patterns taken from two typical individual particles showed only one set of diffraction spots, respectively, suggesting their single-crystal nature (**Figures 2C,D**). HAADF-STEM (**Figure 2E**) and EDX-STEM (**Figures 2F–I**) images, as well as the line-scan profile (**Supplementary Figure S2**) confirmed the core-shell structure and the shell thickness was measured to 5.8 ± 1.9 nm. Despite the sequential addition of Pd and Ag precursor, both Pd and Ag was homogeneously distributed over the shell part, indicating the formation of alloy phase. Instead of showing a multi-layered structure (i.e., Au@Pd@Ag), the ease alloying of Pd and Ag under ambient condition could allow the shell to exhibit the homogenous distribution of both metals. The molar ratio of Au:Pd:Ag was determined by EDS as 81:13:6 (**Supplementary Figure S3**). XPS spectra showed typical doublets for zero-valent Au, Ag and Pd (**Figures 2J–L**). Taken together, we can conclude that the as-obtained products had the Au@PdAg core-shell structure and

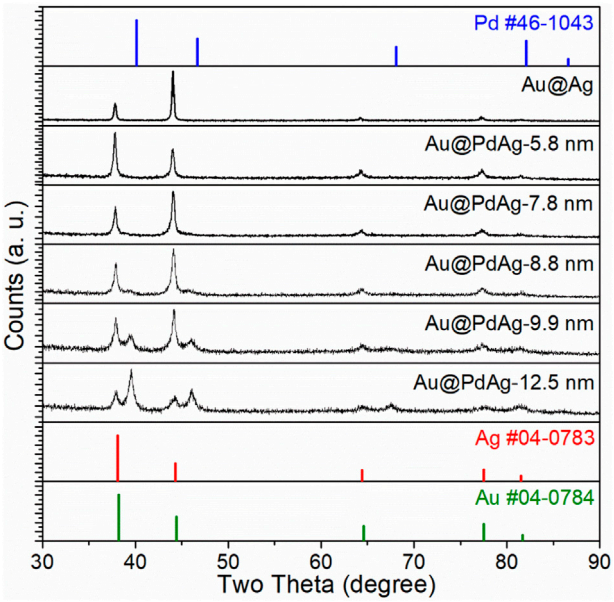

FIGURE 4 | XRD patterns of Au@PdAg core-shell concave nanocubes with different thickness of PdAg shell. Data of Au@Ag core-shell nanocubes and *fcc*-Pd/Ag/Au in JCPDS databased are provided for comparison.

concave cubic morphology, as well as the single-crystal nature and curved surface.

Control Over Shell Thickness

As a major advantage of seeded growth, the PdAg shell thickness could be readily controlled by simply varying the amount of Pd precursor while maintaining other parameters unchanged. As shown in **Figure 3**, the HAADF-STEM and EDX-STEM images clearly showed that PdAg shell noticeably became thicker as more Pd precursor was added, while the overall particle kept the concave cubic morphology despite the change in PdAg shell thickness. In particular, the PdAg shell thickness was measured to be 7.8 ± 3.0, 8.8 ± 3.4, 9.9 ± 4.6, and 12.5 ± 4.9 nm, respectively, when Pd precursor with the amount of 0.2, 0.4, 1, and 2 μmol, respectively, was involved in the growth solution. Line-scan profiles of these products confirmed the core-shell structure and the concave cubic shape, where the Au signal was relatively stronger in the center of the particle and the signal of Pd and Ag mainly emerged at corner/edge regions (**Supplementary Figures S4–S7**). The molar ratio of Au:Pd:Ag for these products were determined using EDS, which were 75:16:9, 74:18:8, 55:30:15, and 40:44:16, respectively (**Supplementary Figures S8–S11**). It is worth noting that the amount of Ag precursor was not varied for all these procedures but the molar ratio of Pd to Ag was roughly maintained at 2:1 in all these products (**Supplementary Figure S12**). It suggested that not all the Ag precursor was reduced and grew on the Au seeds under current synthetic condition and the presence of more Pd precursor would facilitate the seed growth of Ag.

To confirm the presence of PdAg alloy phase, we also took these products with different shell thickness for XRD analyses. As shown in **Figure 4**, the products with the PdAg shell thickness of 5.8 ± 1.9, 7.8 ± 3.0, 8.8 ± 3.4 nm, mainly showed the diffraction peaks of face-centered cubic (*fcc*)-Au phase. The missing of PdAg diffraction peaks for these samples should be attributed to the limited amount of PdAg. As the PdAg shell thickness increased to 9.9 ± 4.6 nm, several diffraction peaks that were located at 39.5°, 46.1°, 67.6°, and 81.4° emerged, right between corresponding (111), (200), (220), and (311) diffraction peaks of Pd and Ag, suggested the formation of PdAg alloy phase. The diffraction peaks of PdAg turned dominant as the shell thickness reached 12.5 ± 4.9 nm, where the diffraction peak intensity of Au became dampened.

Supplementary Figure S13 shows the UV-vis extinction spectra of Au@PdAg concave nanocubes with different shell thickness. For the product with PdAg shell thickness of 5.8 nm, it showed major peak located at 396 nm and a shoulder peak at 508 nm. As the shell became thicker (i.e., 7.8 and 8.8 nm), the major peak shifted to between 500 and 600 nm. Further increase in PdAg shell (i.e., 9.9 and 12.5 nm) caused a broad absorption centered at 616 nm. These results suggested that the plasmonic properties of Au@PdAg core-shell nanocrystals can be tuned by varying the shell thickness and the major absorbance peak can still be observed in the UV-vis extinction spectrum if the thickness was controlled to sub-10 nm range.

Effect of Capping Effect and Reaction Kinetics on Product Morphology

To the elucidate the formation mechanism of PdAg shell with a unique morphology of concave cube, control experiments were conducted to investigated the effect of capping agent and reaction kinetics on product morphology. As shown in **Figures 5A,B**, when the capping agent was replaced by CTAC, the resultant products still exhibited the concave feature but the cubic shape largely lost. It showed that alkyl chain length of quaternary ammonium surfactant played a more crucial role in determining the shape of final products. Contrarily, the use of CTAB led to the formation of products anchored with lots of tiny particles on the surface. Such variation could be attributed to the stronger affinity of the Br^- ions to the Au seeds surface (Zhu et al., 2013), which made it difficult for PdAg atoms to deposit *via* the layer-by-layer mode (Frank-van de Merwe mode). Considering the lattice mismatch between Au and PdAg, the PdAg atoms may tend to form tiny particles on the seed surface to minimize the interfacial energy (Vollmer-Weber mode) (Peng and Hong, 2009).

In addition to the capping agent, the effect of reaction kinetics was also investigated by increasing the amount of reductant in the growth solution. As shown in **Figures 5C,D**, as the amount of AA increased from 5 to 20 μmol and 100 μmol, respectively, the quantity of self-nucleated particles increased in the final products. It could be attributed to the competition between heterogenous and homogeneous nucleation and growth. It is more likely for heterogenous nucleation and growth to occur when the concentration of metallic atoms was controlled to a low level. This is because for homogeneous nucleation, the concentration of

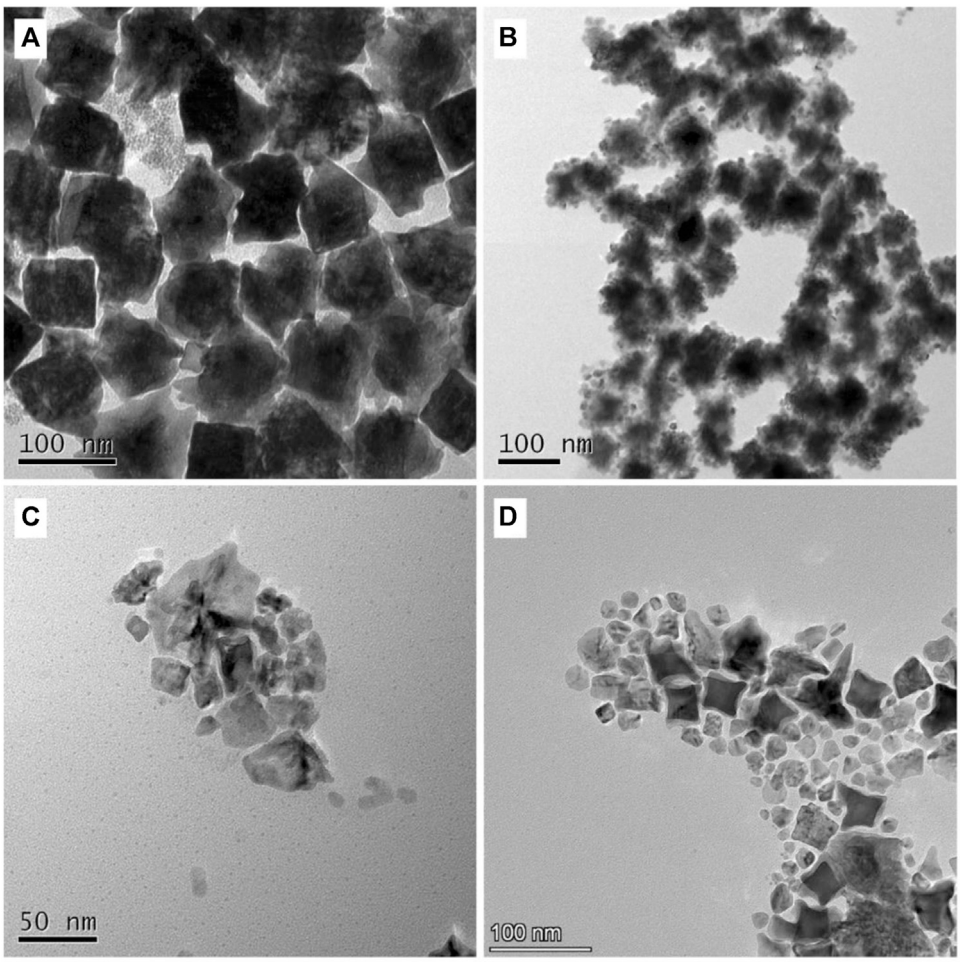

FIGURE 5 | Effect of **(A, B)** capping effect and **(C, D)** reaction kinetics over the product morphology and structure. TEM images of products obtained *via* the synthetic procedure P5, except that **(A, B)** the capping agent DTAC was replaced by **(A)** CTAC and **(B)** CTAB; **(C, D)** the amount of AA was varied from 5 μmol to **(C)** 20 μmol and **(D)** 100 μmol, respectively.

the Pd/Ag atoms should go beyond the supersaturation point (e.g., critical nucleation concentration) to cross the energy barrier (Hsia et al., 2018; Gamler et al., 2020; Liu and Zhang, 2020). Typically, the use of excessive reductant can cause the significant increase in the concentration of newly-formed zero-valent atoms in the growth solution (Zhang et al., 2018). To this end, the generation of Pd/Ag atoms in large quantity within a short time period would make the nucleation and growth dominated by the homogenous route considering the lattice mismatch existed. Without the regulation of seeds, the resulting products would take random shapes and crystallinities. In short, the use of adequate reductant and Br^--free quaternyammonium surfactant contributed to the conformal growth of PdAg over concave cubic Au seeds in the current study.

Electrochemical Measurement

Due to the combined advantage in both structure and elemental composition, the current Au@PdAg core-shell concave nanocubes are expected to find important use as electrocatalysts for EOR in alkaline media. In particular, the product with the 12.5-nm shell thickness was chosen for the dominant phase of PdAg. They were collected *via* centrifugation and loaded on carbon black to construct Au@PdAg/C electrocatalysts. Prior to EOR measurements, the catalysts were washed with water once to remove the residual surfactant for surface purification. For comparison, carbon-supported Au@Pd core-shell nanoparticles and commercial Pd/C electrocatalysts were employed as the reference materials.

As shown in **Supplementary Figure S14**, CV curves collected in 1 M KOH exhibited a pronounced cathode peak between −0.5 and −0.1 V during the backward sweep corresponding to the reduction of surface PdO to metallic Pd. Based on the integrated charge associated with this cathodic peak, we estimated that the electrochemically active surface area (ECSA) of Au@PdAg/C, Au@Pd/C, and Pd/C was 28.50, 30.67, and 161.7 m^2 g_{Pd}^{-1}, respectively. Compared to the commercial Pd/C, the relatively small ECSA values of Au@PdAg/C and Au@Pd/C electrocatalysts could be attributed to the large overall particle size. With the presence of ethanol, all CV curves were drastically changed to

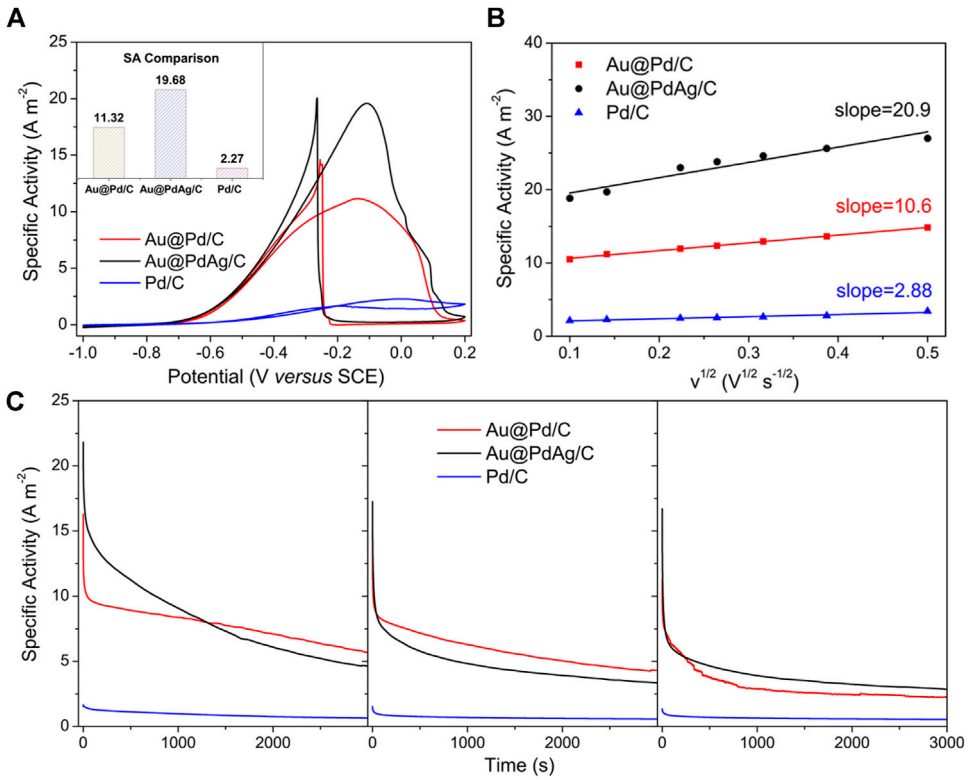

FIGURE 6 | Electrochemical measurements of carbon-supported Au@PdAg concave nanocubes (shell thickness: 12.5 nm, molar ratio: Au:Pd:Ag = 40:44:16) electrocatalysts for EOR: **(A)** CV curves in 1 M ethanol containing 1 M KOH; **(B)** EOR kinetics based on specific activity and scan rates; **(C)** Chronoamperometric stability curves measured at −0.2 V vs. SCE. Data of carbon-supported Au@Pd nanoparticles and commercial Pd/C was provided as reference.

TABLE 2 | Summary of EOR performance of electrocatalysts in the present study.

Electrocatalyst	E_s[a]	E_p[a]	ECSA ($m^2\ g_{Pd}^{-1}$)	j_r/j_f	MA ($mA\ mg_{Pd}^{-1}$)	SA ($A\ m^{-2}$)	*j*(t = 3000s) ($A\ m^{-2}$)		
							1st	2nd	3rd
Au@Pd	−734 mV	−135 mV	28.50	1.31	317.49	11.32	5.66	4.28	2.25
Au@PdAg	−768 mV	−110 mV	30.67	1.02	600.21	19.68	4.62	3.34	2.84
Pd/C	−678 mV	−1 mV	161.7	0.72	367.67	2.27	0.64	0.57	0.54

[a]*E_s, onset potential vs. SCE; E_p, peak potential vs. SCE; MA, mass activity; SA, specific activity.*

have a strong peak in the forward scan due to EOR electrocatalysis (**Figure 6A**). The mass activity and specific activity of Au@PdAg/C was calculated to be 600.21 mA mg_{Pd}^{-1} and 19.57 A m^{-2}, which were both larger than that of Au@Pd/C (317.49 mA mg_{Pd}^{-1} and 11.32 A m^{-2}), and Pd/C (367.67 mA mg_{Pd}^{-1} and 2.27 A m^{-2}). Furthermore, the onset potential (E_s) for the EOR over Au@PdAg/C was −768 mV, which were more negative than that of the Au@Pd/C (−734 mV) and Pd/C (−678 mV) electrocatalyst. It indicated that the electroxidation of ethanol can occur more easily on the Au@PdAg electrocatalyst.

The electrocatalytic kinetics of EOR were also compared to further explore the oxidation process on the surface of the different catalysts. As shown in **Figures 6A,B** linear relationship between the square root of the scan rate ($v^{1/2}$) (30–200 mV s^{-1}) and the forward peak current density could be observed in all three nanomaterials (**Supplementary Figure S15**), indicating a diffusion-controlled process for the EOR (Sun et al., 2012). In addition, the Au@PdAg/C exhibited the enhanced electrocatalytic kinetics as can be concluded from the larger slope value when compared to the Au@Pd/C and Pd/C. All these values imply that the current Au@PdAg/C electrocatalysts have a higher intrinsic electrocatalytic activity for the EOR as compared to Au@Pd/C and Pd/C. In addition, the long-term durability was evaluated *via* three successive cycles of current-time (*i-t*) chronoamperometry measurements at a potential of −0.2 V vs. SCE for 3,000 s. The Au@PdAg/C electrocatalysts manifested a larger residual activity for each cycle as compared to the other two electrocatalysts (**Figure 6C**).

All the as-mentioned data was summarized in **Table 2** for comparison.

The morphology and structure of Au@PdAg/C electrocatalyst after the CA measurements were characterized using electron microscope. As shown in **Supplementary Figure S16**, the electrocatalyst particles were still isolated from each other and no significant agglomeration was noticed (**Supplementary Figure S16A**). The morphology of the PdAg shell over the Au seed varied with some branching feature. Some of the PdAg shells became disengaged from the Au seed surface but their curved surface maintained (**Supplementary Figure S16B**). By conducting analysis using HAADF-STEM (**Supplementary Figure S16C**) and EDX-STEM (**Supplementary Figure S16D**), despite of the reservation of core-shell structure, the alloying between Au and PdAg was observed. The change in morphology and structure of Au@PdAg/C electrocatalysts should be caused by the long-term cycling test, which also explained the decline in ending-point specific activity for each test.

To evaluate the reusability of catalysts, we also conducted three consecutive CA measurements of EOR using Au@PdAg/C electrocatalyst, where the fresh aqueous solution of 1M KOH+1M ethanol was used as the electrolyte for each cycle. As shown in **S upplementary Figure S17**, the specific activity maintained at 3.1, 2.5, and 2.1 A m^{-2} for the consecutive three cycles, respectively, demonstrating the acceptable reusability of the current product for EOR electrocatalysis. In short, owing to the synergistic structural (i.e., stepped facets on the surface) and compositional advantages (i.e., containing both Pd and Ag), the current Au@PdAg nanocrystals exhibited remarkable specific activity, long-term stability, and enhanced electrocatalytic kinetics for EOR in alkaline media.

Compared to commercial Pd/C electrocatalyst, the principal drawbacks of the current products could be mainly attributed to the relatively higher j_r/j_f value (e.g., 0.72 for Pd/C and 1.02 for Au@PdAg/C, **Table 2**), suggesting their weaker ability to poisoning-resistance of the electrodes for ethanol oxidation. It should be caused by its elemental composition, where the doping of Pd with Ag changed the electronic state and the surface affinity towards reaction intermediates. This disadvantage has also been noted in previous studies on PdAg-based EOR electrocatalysts (Li et al., 2014; Fu et al., 2015).

CONCLUSION

In summary, we have successfully prepared Au@PdAg core-shell nanocrystals in the form of concave nanocube by conducting sequential conformal deposition of Pd and Ag over concave cubic Au seeds *via* seeded growth. The thickness of PdAg shell could be tuned in the range of 5–13 nm by simply varying the metallic precursor in growth solution without causing noticeable morphology change to the whole particle. The carbon-supported Au@PdAg core-shell concave nanocubes exhibited superb electrochemical activity (e.g., 600.21 mA mg_{Pd}^{-1} in mass activity and 19.57 A m^{-2} in specific activity), together with improved EOR kinetics and long-term durability, as compared to carbon-supported Au@Pd nanoparticles and commercial Pd/C. The current work offers a feasible strategy to producing bimetallic nanocrystals with concave surface, which could be extended to morphology engineering of other noble-metal nanocrystals for a broad range of applications. It also contributes to the rational design of advanced EOR electrocatalysts with controlled shapes and the current products could find the important practical use for fuel cells and other related energy conversion devices.

DATA AVAILABILITY STATEMENT

The original contributions presented in the study are included in the article/**Supplementary Material**, further inquiries can be directed to the corresponding authors.

AUTHOR CONTRIBUTIONS

YZ: Methodology; Supervision, Writing-original draft, Funding acquisition; YM: Project Administration, Writing-review and editing; QW and GZ: Data curation, Investigation, Funding acquisition; NZ and FL: Formal Analysis; ML: Resources.

FUNDING

This work was financially supported by the Natural Science Foundation of China (Grant No. 21701100), Key Research and Development Project of Shandong Province (Grant No. 2019GGX102081), Key Research and Development Project of Jining (Grant No. 2019ZDGH026), Young Innovative Talents Introduction and Cultivation Program for Colleges and Universities of Shandong Province (Granted by Department of Education of Shandong Province, Sub-Title: Innovative Research Team on Optoelectronic Functional Materials), and Doctoral Startup Research Funding of Jining University (Grant No. 2020BSZX01) and Distinguished Hundred Talent Program (Grant No. 2020ZYRC05) of Jining University. This work is also supported by the open project (Grant No. KS 2022) of Jiangsu Key Laboratory for Carbon-Based Functional Materials and Devices (Soochow University), Collaborative Innovation Center of Suzhou Nano Science and Technology, the Priority Academic Program Development of Jiangsu Higher Education Institutions (PAPD), the 111 Project, Joint International Research Laboratory of Carbon-Based Functional Materials and Devices.

SUPPLEMENTARY MATERIAL

The Supplementary Material for this article can be found online at: https://www.frontiersin.org/articles/10.3389/fmats.2021.761236/full#supplementary-material

REFERENCES

An, L., and Zhao, T. S. (2011). An Alkaline Direct Ethanol Fuel Cell with a Cation Exchange Membrane. *Energy Environ. Sci.* 4 (6), 2213–2217. doi:10.1039/C1EE00002K

Antolini, E. (2007). Catalysts for Direct Ethanol Fuel Cells. *J. Power Sourc.* 170 (1), 1–12. doi:10.1016/j.jpowsour.2007.04.009

Bin, D., Yang, B., Zhang, K., Wang, C., Wang, J., Zhong, J., et al. (2016). Design of PdAg Hollow Nanoflowers through Galvanic Replacement and Their Application for Ethanol Electrooxidation. *Chem. Eur. J.* 22 (46), 16642–16647. doi:10.1002/chem.201601544

Cui, Z., Hu, J., Jiang, X., Zhang, D., and Fang, C. (2021). Asymmetric Au/(PdAg alloy) Nano-Allium Giganteums for Their Enhanced Electrocatalytic Performances to Ethanol Oxidation Reaction. *J. Alloys Compd.* 855, 157385. doi:10.1016/j.jallcom.2020.157385

Dutta, S., Ray, C., Sasmal, A. K., Negishi, Y., and Pal, T. (2016). Fabrication of Dog-Bone Shaped Au NRcore-Pt/Pdshell Trimetallic Nanoparticle-Decorated Reduced Graphene Oxide Nanosheets for Excellent Electrocatalysis. *J. Mater. Chem. A.* 4 (10), 3765–3776. doi:10.1039/C6TA00379F

Fang, C., Zhao, G., Zhang, Z., Zheng, J., Ding, Q., Xu, X., et al. (2018). Morphology Engineering of Au/(PdAg Alloy) Nanostructures for Enhanced Electrocatalytic Ethanol Oxidation. *Part. Part. Syst. Charact.* 35 (10), 1800258. doi:10.1002/ppsc.201800258

Feng, Y.-Y., Liu, Z.-H., Xu, Y., Wang, P., Wang, W.-H., and Kong, D.-S. (2013). Highly Active PdAu alloy Catalysts for Ethanol Electro-Oxidation. *J. Power Sourc.* 232, 99–105. doi:10.1016/j.jpowsour.2013.01.013

Fu, S., Zhu, C., Du, D., and Lin, Y. (2015). Facile One-step Synthesis of Three-Dimensional Pd-Ag Bimetallic Alloy Networks and Their Electrocatalytic Activity toward Ethanol Oxidation. *ACS Appl. Mater. Inter.* 7 (25), 13842–13848. doi:10.1021/acsami.5b01963

Fu, X., Wan, C., Zhang, A., Zhao, Z., Huyan, H., Pan, X., et al. (2020). Pt3Ag alloy Wavy Nanowires as Highly Effective Electrocatalysts for Ethanol Oxidation Reaction. *Nano Res.* 13 (5), 1472–1478. doi:10.1007/s12274-020-2754-4

Gamler, J. T. L., Leonardi, A., Sang, X., Koczkur, K. M., Unocic, R. R., Engel, M., et al. (2020). Effect of Lattice Mismatch and Shell Thickness on Strain in Core@shell Nanocrystals. *Nanoscale Adv.* 2 (3), 1105–1114. doi:10.1039/D0NA00061B

Gilroy, K. D., Ruditskiy, A., Peng, H.-C., Qin, D., and Xia, Y. (2016). Bimetallic Nanocrystals: Syntheses, Properties, and Applications. *Chem. Rev.* 116 (18), 10414–10472. doi:10.1021/acs.chemrev.6b00211

Hong, W., Wang, J., and Wang, E. (2014). Facile Synthesis of Highly Active PdAu Nanowire Networks as Self-Supported Electrocatalyst for Ethanol Electrooxidation. *ACS Appl. Mater. Inter.* 6 (12), 9481–9487. doi:10.1021/am501859k

Hong, Y., Kim, H. J., Lee, H. J., Kim, J., and Choi, S.-I. (2019). Ni(OH)2 Decorated Pt-Cu Octahedra for Ethanol Electrooxidation Reaction. *Front. Chem.* 7, 608. doi:10.3389/fchem.2019.00608

Hsia, C.-F., Chang, C.-H., and Huang, M. H. (2018). Unusually Large Lattice Mismatch-Induced Optical Behaviors of Au@Cu-Cu2 O Core-Shell Nanocrystals with Noncentrally Located Cores. *Part. Part. Syst. Charact.* 35 (7), 1800112. doi:10.1002/ppsc.201800112

Hu, C., Zhai, X., Zhao, Y., Bian, K., Zhang, J., Qu, L., et al. (2014). Small-sized PdCu Nanocapsules on 3D Graphene for High-Performance Ethanol Oxidation. *Nanoscale* 6 (5), 2768–2775. doi:10.1039/C3NR05722D

Huang, W., Kang, X., Xu, C., Zhou, J., Deng, J., Li, Y., et al. (2018). 2D PdAg Alloy Nanodendrites for Enhanced Ethanol Electroxidation. *Adv. Mater.* 30 (11), 1706962. doi:10.1002/adma.201706962

Ishimoto, T., Ogura, T., Koyama, M., Yang, L., Kinoshita, S., Yamada, T., et al. (2013). A Key Mechanism of Ethanol Electrooxidation Reaction in a Noble-Metal-Free Metal-Organic Framework. *J. Phys. Chem. C* 117 (20), 10607–10614. doi:10.1021/jp4031046

Jana, R., Datta, A., and Malik, S. (2021). Tuning Intermediate Adsorption in Structurally Ordered Substituted PdCu3 Intermetallic Nanoparticles for Enhanced Ethanol Oxidation Reaction. *Chem. Commun.* 57 (37), 4508–4511. doi:10.1039/D0CC08075F

Jiang, K., Wang, P., Guo, S., Zhang, X., Shen, X., Lu, G., et al. (2016). Ordered PdCu-Based Nanoparticles as Bifunctional Oxygen-Reduction and Ethanol-Oxidation Electrocatalysts. *Angew. Chem. Int. Ed.* 55 (31), 9030–9035. doi:10.1002/anie.201603022

Jo, Y.-G., Kim, S.-M., Kim, J.-W., and Lee, S.-Y. (2016). Composition-tuned Porous Pd-Ag Bimetallic Dendrites for the Enhancement of Ethanol Oxidation Reactions. *J. Alloys Compd.* 688, 447–453. doi:10.1016/j.jallcom.2016.07.227

Kabiraz, M. K., Kim, J., and Choi, S. I. (2021). Shape and Hydriding Effects of Palladium Nanocatalyst toward Oxygen Electroreduction Reaction. *Bull. Korean Chem. Soc.* 42 (5), 802–805. doi:10.1002/bkcs.12183

Kim, J., Kim, H., Lee, W.-J., Ruqia, B., Baik, H., Oh, H.-S., et al. (2019). Theoretical and Experimental Understanding of Hydrogen Evolution Reaction Kinetics in Alkaline Electrolytes with Pt-Based Core-Shell Nanocrystals. *J. Am. Chem. Soc.* 141 (45), 18256–18263. doi:10.1021/jacs.9b09229

Kim, H. J., Ahn, Y.-D., Kim, J., Kim, K.-S., Jeong, Y. U., Hong, J. W., et al. (2020). Surface Elemental Distribution Effect of Pt-Pb Hexagonal Nanoplates for Electrocatalytic Methanol Oxidation Reaction. *Chin. J. Catal.* 41 (5), 813–819. doi:10.1016/S1872-2067(19)63310-3

Kuo, C.-S., Kao, C.-R., Chen, W.-J., Lu, M.-Y., Cullen, D. A., Sneed, B. T., et al. (2018). Aqueous Synthesis of Concave Rh Nanotetrahedra with Defect-Rich Surfaces: Insights into Growth-, Defect-, and Plasmon-Enhanced Catalytic Energy Conversion. *Chem. Mater.* 30 (13), 4448–4458. doi:10.1021/acs.chemmater.8b02003

Lahiri, A., and Endres, F. (2017). Review-Electrodeposition of Nanostructured Materials from Aqueous, Organic and Ionic Liquid Electrolytes for Li-Ion and Na-Ion Batteries: A Comparative Review. *J. Electrochem. Soc.* 164 (9), D597–D612. doi:10.1149/2.1011709jes

Lahiri, A., Chutia, A., Carstens, T., and Endres, F. (2020). Surface-Oxygen Induced Electrochemical Self-Assembly of Mesoporous Conducting Polymers for Electrocatalysis. *J. Electrochem. Soc.* 167 (11), 112501. doi:10.1149/1945-7111/ab9e3c

Lamy, C., Belgsir, E. M., and Léger, J.-M. (2001). Electrocatalytic Oxidation of Aliphatic Alcohols: Application to the Direct Alcohol Fuel Cell (DAFC). *J. Appl. Electrochem.* 31 (7), 799–809. doi:10.1023/A:1017587310150

Langille, M. R., Personick, M. L., Zhang, J., and Mirkin, C. A. (2012). Defining Rules for the Shape Evolution of Gold Nanoparticles. *J. Am. Chem. Soc.* 134 (35), 14542–14554. doi:10.1021/ja305245g

Li, G., Jiang, L., Jiang, Q., Wang, S., and Sun, G. (2011). Preparation and Characterization of PdxAgy/C Electrocatalysts for Ethanol Electrooxidation Reaction in Alkaline media. *Electrochim. Acta* 56 (22), 7703–7711. doi:10.1016/j.electacta.2011.06.036

Li, Z., Yang, L., Li, Y., Yang, Y., Zhou, C., Ding, Y., et al. (2013). Effects of Pore Size on the Mechanical Properties of Three-Dimensionally Ordered Macroporous Nickel. *Mater. Des.* 45, 52–55. doi:10.1016/j.matdes.2012.09.009

Li, L., Chen, M., Huang, G., Yang, N., Zhang, L., Wang, H., et al. (2014). A green Method to Prepare Pd-Ag Nanoparticles Supported on Reduced Graphene Oxide and Their Electrochemical Catalysis of Methanol and Ethanol Oxidation. *J. Power Sourc.* 263, 13–21. doi:10.1016/j.jpowsour.2014.04.021

Liang, Z. X., Zhao, T. S., Xu, J. B., and Zhu, L. D. (2009). Mechanism Study of the Ethanol Oxidation Reaction on Palladium in Alkaline media. *Electrochim. Acta* 54 (8), 2203–2208. doi:10.1016/j.electacta.2008.10.034

Liu, J., and Zhang, J. (2020). Nanointerface Chemistry: Lattice-Mismatch-Directed Synthesis and Application of Hybrid Nanocrystals. *Chem. Rev.* 120 (4), 2123–2170. doi:10.1021/acs.chemrev.9b00443

Liu, H., Adzic, R. R., and Wong, S. S. (2015). Multifunctional Ultrathin PdxCu1-X and Pt~PdxCu1-X One-Dimensional Nanowire Motifs for Various Small Molecule Oxidation Reactions. *ACS Appl. Mater. Inter.* 7 (47), 26145–26157. doi:10.1021/acsami.5b07964

Liu, J., Luo, Z., Li, J., Yu, X., Llorca, J., Nasiou, D., et al. (2019). Graphene-supported Palladium Phosphide PdP2 Nanocrystals for Ethanol Electrooxidation. *Appl. Catal. B: Environ.* 242, 258–266. doi:10.1016/j.apcatb.2018.09.105

Lu, Y., and Chen, W. (2012). PdAg Alloy Nanowires: Facile One-step Synthesis and High Electrocatalytic Activity for Formic Acid Oxidation. *ACS Catal.* 2 (1), 84–90. doi:10.1021/cs200538g

Luo, Z., Ahn, J., and Qin, D. (2019). Fabrication of Ag-Pd Concave Nanocrystals through Facet-Selective Oxidation of Ag Atoms. *Nanoscale* 11 (14), 6710–6718. doi:10.1039/C9NR01250H

Lv, H., Wang, Y., Lopes, A., Xu, D., and Liu, B. (2019). Ultrathin PdAg Single-Crystalline Nanowires Enhance Ethanol Oxidation Electrocatalysis. *Appl. Catal. B: Environ.* 249, 116–125. doi:10.1016/j.apcatb.2019.02.068

Lv, H., Teng, Y., Wang, Y., Xu, D., and Liu, B. (2020). Highly Branched and Defect-Rich PdP Nanosheets for Ethanol Oxidation Electrocatalysis. *Chem. Commun.* 56 (100), 15667–15670. doi:10.1039/D0CC06725C

Mann, J., Yao, N., and Bocarsly, A. B. (2006). Characterization and Analysis of New Catalysts for a Direct Ethanol Fuel Cell. *Langmuir* 22 (25), 10432–10436. doi:10.1021/la061200c

Nguyen, M. T. X., Nguyen, M.-K., Pham, P. T. T., Huynh, H. K. P., and Nguyen, S. T. (2021). Pd Coated One-Dimensional Ag Nanostructures: Controllable Architecture and Their Electrocatalytic Performance for Ethanol Oxidation in Alkaline media. *Int. J. Hydrogen Energ.* 46 (5), 3909–3921. doi:10.1016/j.ijhydene.2020.10.226

Peng, Z., and Yang, H. (2009). Designer Platinum Nanoparticles: Control of Shape, Composition in alloy, Nanostructure and Electrocatalytic Property. *Nano Today* 4 (2), 143–164. doi:10.1016/j.nantod.2008.10.010

Peng, C., Hu, Y., Liu, M., and Zheng, Y. (2015). Hollow Raspberry-like PdAg alloy Nanospheres: High Electrocatalytic Activity for Ethanol Oxidation in Alkaline media. *J. Power Sourc.* 278, 69–75. doi:10.1016/j.jpowsour.2014.12.056

Shen, S. Y., Zhao, T. S., and Wu, Q. X. (2012). Product Analysis of the Ethanol Oxidation Reaction on Palladium-Based Catalysts in an Anion-Exchange Membrane Fuel Cell Environment. *Int. J. Hydrogen Energ.* 37 (1), 575–582. doi:10.1016/j.ijhydene.2011.09.077

Stein, A., Li, F., and Denny, N. R. (2008). Morphological Control in Colloidal Crystal Templating of Inverse Opals, Hierarchical Structures, and Shaped Particles. *Chem. Mater.* 20 (3), 649–666. doi:10.1021/cm702107n

Sun, J., Wang, Y., Zhang, C., Kou, T., and Zhang, Z. (2012). Anodization Driven Enhancement of Catalytic Activity of Pd towards Electro-Oxidation of Methanol, Ethanol and Formic Acid. *Electrochemistry Commun.* 21, 42–45. doi:10.1016/j.elecom.2012.04.023

Tian, N., Zhou, Z.-Y., Sun, S.-G., Ding, Y., and Wang, Z. L. (2007). Synthesis of Tetrahexahedral Platinum Nanocrystals with High-Index Facets and High Electro-Oxidation Activity. *Science* 316 (5825), 732–735. doi:10.1126/science.1140484

Tsuji, M., Takemura, K., Shiraishi, C., Ikedo, K., Uto, K., Yajima, A., et al. (2015). Syntheses of Au@PdAg and Au@PdAg@Ag Core-Shell Nanorods through Distortion-Induced Alloying between Pd Shells and Ag Atoms over Au Nanorods. *J. Phys. Chem. C* 119 (20), 10811–10823. doi:10.1021/jp509340s

Wang, H., Jusys, Z., and Behm, R. J. (2004). Ethanol Electrooxidation on a Carbon-Supported Pt Catalyst: Reaction Kinetics and Product Yields. *J. Phys. Chem. B* 108 (50), 19413–19424. doi:10.1021/jp046561k

Wang, K.-W., Kang, W.-D., Wei, Y.-C., Liu, C.-W., Su, P.-C., Chen, H.-S., et al. (2012). Promotion of PdCu/C Catalysts for Ethanol Oxidation in Alkaline Solution by SnO2Modifier. *ChemCatChem* 4 (8), 1154–1161. doi:10.1002/cctc.201100500

Wang, W., Lv, F., Lei, B., Wan, S., Luo, M., and Guo, S. (2016). Tuning Nanowires and Nanotubes for Efficient Fuel-Cell Electrocatalysis. *Adv. Mater.* 28 (46), 10117–10141. doi:10.1002/adma.201601909

Wang, W., Zhang, X., Zhang, Y., Chen, X., Ye, J., Chen, J., et al. (2020). Edge Enrichment of Ultrathin 2D PdPtCu Trimetallic Nanostructures Effectuates Top-Ranked Ethanol Electrooxidation. *Nano Lett.* 20 (7), 5458–5464. doi:10.1021/acs.nanolett.0c01908

Wang, H., Zhou, T., Mao, Q., Wang, S., Wang, Z., Xu, Y., et al. (2021). Porous PdAg alloy Nanostructures with a Concave Surface for Efficient Electrocatalytic Methanol Oxidation. *Nanotechnology* 32 (35), 355402. doi:10.1088/1361-6528/ac0471

Xia, X., Zeng, J., McDearmon, B., Zheng, Y., Li, Q., and Xia, Y. (2011). Silver Nanocrystals with Concave Surfaces and Their Optical and Surface-Enhanced Raman Scattering Properties. *Angew. Chem. Int. Ed.* 50 (52), 12542–12546. doi:10.1002/anie.201105200

Yang, Z.-Z., Liu, L., Wang, A.-J., Yuan, J., Feng, J.-J., and Xu, Q.-Q. (2017). Simple Wet-Chemical Strategy for Large-Scaled Synthesis of snowflake-like PdAu alloy Nanostructures as Effective Electrocatalysts of Ethanol and Ethylene Glycol Oxidation. *Int. J. Hydrogen Energ.* 42 (4), 2034–2044. doi:10.1016/j.ijhydene.2016.08.088

Yang, W., Wang, H., and Fu, F. (2019). PdCu Nanoalloys Deposited on Porous Carbon as a Highly Efficient Catalyst for Ethanol Oxidation. *Mater. Chem. Phys.* 228, 175–179. doi:10.1016/j.matchemphys.2019.02.075

Yang, M., Lao, X., Sun, J., Ma, N., Wang, S., Ye, W., et al. (2020a). Assembly of Bimetallic PdAg Nanosheets and Their Enhanced Electrocatalytic Activity toward Ethanol Oxidation. *Langmuir* 36 (37), 11094–11101. doi:10.1021/acs.langmuir.0c02102

Yang, X., Liang, Z., Chen, S., Ma, M., Wang, Q., Tong, X., et al. (2020b). A Phosphorus-Doped Ag@Pd Catalyst for Enhanced C-C Bond Cleavage during Ethanol Electrooxidation. *Small* 16 (47), 2004727. doi:10.1002/smll.202004727

You, H., Gao, F., Song, T., Zhang, Y., Wang, H., Liu, X., et al. (2020). Tunable Long-Chains of Core@shell PdAg@Pd as High-Performance Catalysts for Ethanol Oxidation. *J. Colloid Interf. Sci.* 574, 182–189. doi:10.1016/j.jcis.2020.04.051

Yu, Y., Zhang, Q., Lu, X., and Lee, J. Y. (2010). Seed-Mediated Synthesis of Monodisperse Concave Trisoctahedral Gold Nanocrystals with Controllable Sizes. *J. Phys. Chem. C* 114 (25), 11119–11126. doi:10.1021/jp103840k

Yu, X., Liu, J., Li, J., Luo, Z., Zuo, Y., Xing, C., et al. (2020). Phosphorous Incorporation in Pd2Sn Alloys for Electrocatalytic Ethanol Oxidation. *Nano Energy* 77, 105116. doi:10.1016/j.nanoen.2020.105116

Zhang, L., Su, H., Sun, M., Wang, Y., Wu, W., Yu, T., et al. (2015). Concave Cu-Pd Bimetallic Nanocrystals: Ligand-Based Co-reduction and Mechanistic Study. *Nano Res.* 8 (7), 2415–2430. doi:10.1007/s12274-015-0752-8

Zhang, G., Yang, Z., Zhang, W., Hu, H., Wang, C., Huang, C., et al. (2016a). Tailoring the Morphology of Pt3Cu1nanocrystals Supported on Graphene Nanoplates for Ethanol Oxidation. *Nanoscale* 8 (5), 3075–3084. doi:10.1039/C5NR08013D

Zhang, L., Chang, Q., Chen, H., and Shao, M. (2016b). Recent Advances in Palladium-Based Electrocatalysts for Fuel Cell Reactions and Hydrogen Evolution Reaction. *Nano Energy* 29, 198–219. doi:10.1016/j.nanoen.2016.02.044

Zhang, J., Li, H., Kuang, Q., and Xie, Z. (2018). Toward Rationally Designing Surface Structures of Micro- and Nanocrystallites: Role of Supersaturation. *Acc. Chem. Res.* 51 (11), 2880–2887. doi:10.1021/acs.accounts.8b00344

Zhang, G., Ma, Y., Liu, Z., Fu, X., Niu, X., Qu, F., et al. (2020). Seed-Morphology-Directed Synthesis of Concave Gold Nanocrystals with Tunable Sizes. *Langmuir* 36 (51), 15610–15617. doi:10.1021/acs.langmuir.0c03142

Zhao, Y., Maswadeh, Y., Shan, S., Cronk, H., Skeete, Z., Prasai, B., et al. (2017). Composition-Structure-Activity Correlation of Platinum-Ruthenium Nanoalloy Catalysts for Ethanol Oxidation Reaction. *J. Phys. Chem. C* 121 (32), 17077–17087. doi:10.1021/acs.jpcc.7b03901

Zhu, C., Zeng, J., Tao, J., Johnson, M. C., Schmidt-Krey, I., Blubaugh, L., et al. (2012). Kinetically Controlled Overgrowth of Ag or Au on Pd Nanocrystal Seeds: From Hybrid Dimers to Nonconcentric and Concentric Bimetallic Nanocrystals. *J. Am. Chem. Soc.* 134 (38), 15822–15831. doi:10.1021/ja305329g

Zhu, C., Zeng, J., Lu, P., Liu, J., Gu, Z., and Xia, Y. (2013). Aqueous-Phase Synthesis of Single-Crystal Pd Seeds 3 Nm in Diameter and Their Use for the Growth of Pd Nanocrystals with Different Shapes. *Chem. Eur. J.* 19 (16), 5127–5133. doi:10.1002/chem.201203787

Conflict of Interest: The authors declare that the research was conducted in the absence of any commercial or financial relationships that could be construed as a potential conflict of interest.

Publisher's Note: All claims expressed in this article are solely those of the authors and do not necessarily represent those of their affiliated organizations, or those of the publisher, the editors and the reviewers. Any product that may be evaluated in this article, or claim that may be made by its manufacturer, is not guaranteed or endorsed by the publisher.